Journal of Composite Materials OnlineFirst, published on September 9, 2009 as doi:10.1177/0021998309346186

Strengthening of Masonry Walls Using Hybrid-fiber Engineered Cementitious Composite

V. W. J. LIN AND S. T. QUEK*
Department of Civil Engineering, National University of Singapore, Singapore 117576

M. P. NGUYEN
School of Civil and Environmental Engineering
Nanyang Technology University, Singapore 639798

M. MAALEJ
Department of Civil and Environmental Engineering
College of Engineering, University of Sharjah, Sharjah, UAE

ABSTRACT: In this article, the experimental results of hybrid-fiber engineered cementitious composite (HFECC)-strengthened masonry walls subjected to quasi-static out-of-plane loadings are reported. The aim is to assess the extent to which HFECC-strengthening systems can improve the out-of-plane resistance of unreinforced masonry walls. A total of 12 masonry panels were fabricated and tested in the laboratory under both patch load and uniformly distributed load. Test results showed significant improvement of HFECC-strengthened masonry wall's performance against out-of-plane loadings. To provide design aid for such HFECC-strengthened masonry walls, simplified theoretical models were also developed to predict its out-of-plane ultimate load-carrying capacities based on the observed failure mechanisms. The theoretically predicted values compared favorably with experimental data.

KEY WORDS: fiber-reinforced cementitious composites, masonry, strength, load-carrying capacity, out-of-plane loading, analytical model.

INTRODUCTION

MASONRY WALLS ARE generally designed to withstand in-plane compression with little considerations on out-of-plane loadings As such, unreinforced masonry (URM)

*Author to whom correspondence should addressed. E-mail: cveqst@nus.edu.sg
Figures 1, 4–7 and 11 appear in color online: http://jcm.sagepub.com

0021-9983/09/00 0001–23 $10.00/0 DOI: 10.1177/0021998309346186

walls generally fail without structural integrity when they are subjected to accidental out-of-plane loadings, such as a car crashing onto the wall. Traditional methods of strengthening URMs against such loadings include grout injection, stitching, and prestressing [1]. Although these methods are effective in increasing the strength, stiffness, and ductility of URM structures, they generally do not provide sufficient resistance against those accidental loadings.

A more recent strengthening technique developed is the use of fiber-reinforced polymer (FRP) reinforcements for retrofitting existing masonry structures. Studies have been conducted extensively [2–4] to understand the behavior of FRP-strengthening systems. These studies showed that FRP reinforcements could be easily attached onto the masonry wall, increasing its out-of-plane resistance significantly. However, FRP materials generally behave elastically up to the point of failure. As such, masonry walls strengthened with FRP usually fail with little or no ductility. Furthermore, the high retrofitting cost of FRP-strengthening systems made it uneconomical and impractical for civilian structure applications.

The objective of this study is to develop a more effective and economical method for strengthening URM structures. In particular, the application of hybrid-fiber-engineered cementitious composites (HFECC) for strengthening URM walls is investigated.

Over the past decade, a new class of civil engineering materials known as high-performance fiber-reinforced cementitious composites (HPFRCC) has been developed. Engineered cementitious composite (ECC) is a sub-class of HPFRCC engineered by designing the microstructure to obtain extraordinary toughness and ductility [5–7]. ECC has exhibited excellent behavior under tensile, flexural, and shear loading. It has high fracture energy and notch insensitivity, thus making it ideal as a material for various structural applications.

A typical ECC mix contains water, cement, fibers, and some common chemical additives employing a water/cement ratio of 0.5 or lower. Reinforced with relatively low volume (typically $\leq 2\%$) of short randomly distributed discontinuous fibers, the mixing process of ECC is similar to that of normal concrete [8]. In many aspects, ECC has exhibited characteristics similar to medium- to high-strength concrete. Besides having compressive strengths ranging from 30 to 70 MPa (depending on its matrix composition), ECC also has a higher compressive strain capacity of 0.4–0.65% compared to some fiber reinforced concrete (FRC) [5]. The elastic modulus of ECC typically ranges from 18 to 26 GPa, depending largely on the aggregates/fibers used [9–10]. It is worth to mention here that higher elastic modulus of ECC can be achieved without sacrificing its tensile strain-hardening ability by careful control of aggregate content and size [10].

When subjected to tension, ECC exhibits strain-hardening and micro-cracking behavior after first crack. The uni-axial tensile strain capacity of ECC usually exceeds 1% and has values as high as 6–8% with the most ductile composite [8]. In general, ECC has uni-axial tensile strength ranging from 2.5 to 3 MPa at its first crack and ultimate uni-axial tensile strength of 4.5–6 MPa depending on its fiber composite.

Most of the studies carried out on ECC have been on mono-fiber systems such as polyethylene (PE), polyvinyl alcohol (PVA), or steel fibers (ST). Normally, mono-fiber system ECC containing high-modulus fibers (e.g., steel and carbon) exhibit relatively high ultimate strength but low strain capacity, while those containing low-modulus fibers (e.g., PE and PVA) exhibit the opposite behaviors [11]. In a study by Ahmed [12], a HFECC using proper volume ratio of high- and low-modulus fibers was developed to better meet the functional requirement for impact- and blast-resistant structures. This HFECC comprising 0.5% ST fiber and 1.5% PE fiber reinforcements (by volume) was designed to

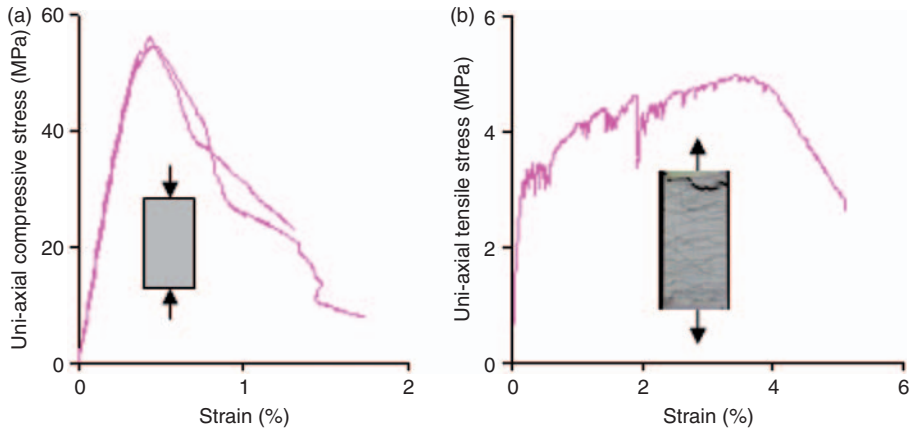

Figure 1. *Typical stress–strain curves of HFECC: (a) uni-axial compression and (b) uni-axial tension.*

achieve an optimal balance between ultimate strength and strain capacity. Typical uni-axial compressive and tensile stress–strain curves of the HFECC material are presented in Figure 1(a) and (b), respectively.

Apart from the mechanical properties of ECC mentioned so-far, recent investigations [13] have verified ECC as an outstanding repair material. It was proven that ductility of repair material is essential for achieving durability in the repaired structure. In particular, ECC have large tensile ductility that relaxes potential stress build-up in the repair layer under drying shrinkage conditions. This behavior was accomplished by the multiple micro-crack damage, which minimizes the delamination at the interface. Therefore, it is expected for HFECC to be a good material for strengthening URM structures against out-of-plane loading.

EXPERIMENTAL INVESTIGATION

A total of 12 masonry panels each measured 1000 mm × 1000 mm in plan and 100 mm in thickness (excluding the HFECC-strengthening layer) were fabricated and tested in the laboratory. Both quasi-static patch load and uniformly distributed load (UDL) were considered. Emphasis of the test was placed on the walls' failure mechanism, structural ductility, and ultimate load-carrying capacity.

Materials

All walls were fabricated using solid clay bricks each having dimensions of 215 mm × 100 mm × 70 mm. The brick units were laid in running bond with mortar layers of approximately 10 mm in thickness. ASTM Type 1 cement and plastering sand were used to prepare the mortar mix, for which the cement: sand proportions were 1 : 3.5 by weight. The constructed masonry walls were then cured under indoor condition for at least 1 week to gain sufficient strength before it was retrofitted with the HFECC-strengthening system.

As mentioned earlier, the HFECC mix used contains 0.5% ST fibers and 1.5% high-performance PE fibers. The ST fibers were supplied by Bekaert Fibre Technologies,

Belgium, while the PE fibers having the trade name Spectra 900, were supplied by MiniFibers, Inc. USA. The properties for the fibers used are shown in Table 1. A total of three 100 mm × 200 mm cylinders and six 300 mm × 75 mm × 15 mm tensile coupons were fabricated to obtain the compressive and the tensile strengths of the HFECC material, respectively.

Auxiliary Material Properties Tests

The compressive cylinder test was carried out in accordance to ASTM C469-02 [14], while the tensile strength of HFECC was obtained using uni-axial tensile test set-up as shown in Figure 2. The loading for the tensile test was applied using displacement control hydraulic jack at a constant rate of 0.1 mm/min.

As the compressive test for the masonry element recommended by the BS5628 design code [15] requires specimens that are larger than the test wall dimensions used in this study, a customized compressive test was designed to determine the in-plane compressive stress–strain relationship of the masonry unit for both directions, normal and parallel to the mortar bed joint. Masonry wallettes having dimensions of 230 mm × 330 mm × 100 mm were loaded to failure in the test set-up shown in Figure 3. The strain of the masonry unit was measured by taking the average readings of four LVDTs, located in all four sides, divided by

Table 1. Properties of fibers used.

Fiber type	Length (mm)	Diameter (μm)	Young's modulus (GPa)	Tensile strength (MPa)
Steel	13	200	200	2500
Polyethylene	12	39	66	2610

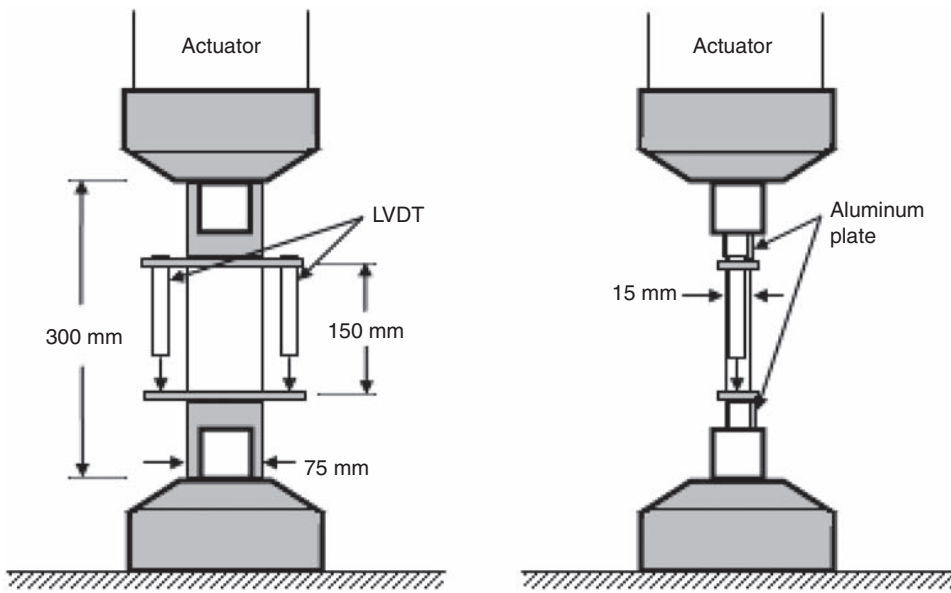

Figure 2. *Plan view and side view of tensile coupon test.*

the specimen gauge length which was taken as 150 mm. Six 100 mm masonry cubes were fabricated by cutting larger masonry specimens into the required size to investigate its out-of-plane compressive strength.

In addition, the interfacial shear bond strength and the uni-axial tensile-bond strength between HFECC material and masonry wall were also investigated through a direct shear test and uni-axial tensile-bond test as shown in Figure 4(a) and (b), respectively.

Wall Specimens

The test walls were grouped into two series, with Series I focusing on patch load and Series II focusing on UDL. Each series of test consisted of two URM walls serving as control specimen and four HFECC-strengthened masonry walls. The four strengthening configurations studied were namely, (1) single-face of 34 mm-thick HFECC-strengthening layer (SE34), (2) double-face of 34 mm-thick HFECC-strengthening layer (DE34) each, (3) single-face of 34 mm-thick HFECC-strengthening layer with 8 mm-diameter steel mesh (SD8), and (4) double-face of 34 mm-thick HFECC-strengthening layer with 8 mm-diameter steel mesh (DD8) each as summarized in Table 2. The steel reinforcement ratios including both ST fibers and steel mesh of each specimen are also shown. Each strengthened wall panel is differentiated using a combination of four to five characters. The first alphabet, P (Patch) or U (Uniformly distributed) refers to the type of loading and the following three or four characters refer to the reinforcement configurations as described above.

Retrofitting URM Walls with HFECC-strengthening System

To simulate actual site conditions, the HFECC-strengthening layer was plastered onto the masonry walls vertically instead of laying the wall down and cast on it horizontally. The masonry wall surface was first wetted to minimize it from dehydrating the HFECC-strengthening layer and the 34 mm thick HFECC layer was then plastered onto the wall in two layers to minimize sagging effects due to its self-weight. The strengthened masonry walls were covered up with moistened gunnysack to cure the HFECC layer for 28 days before testing.

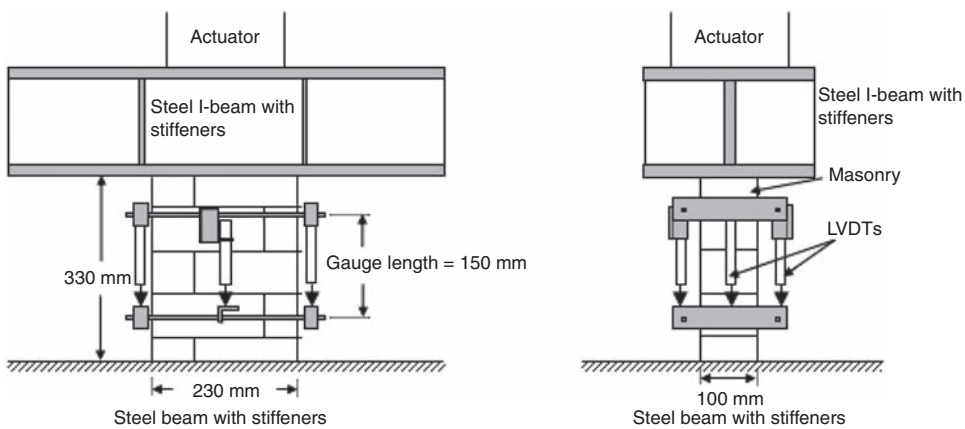

Figure 3. *Plan view and side view of masonry wallette compression test.*

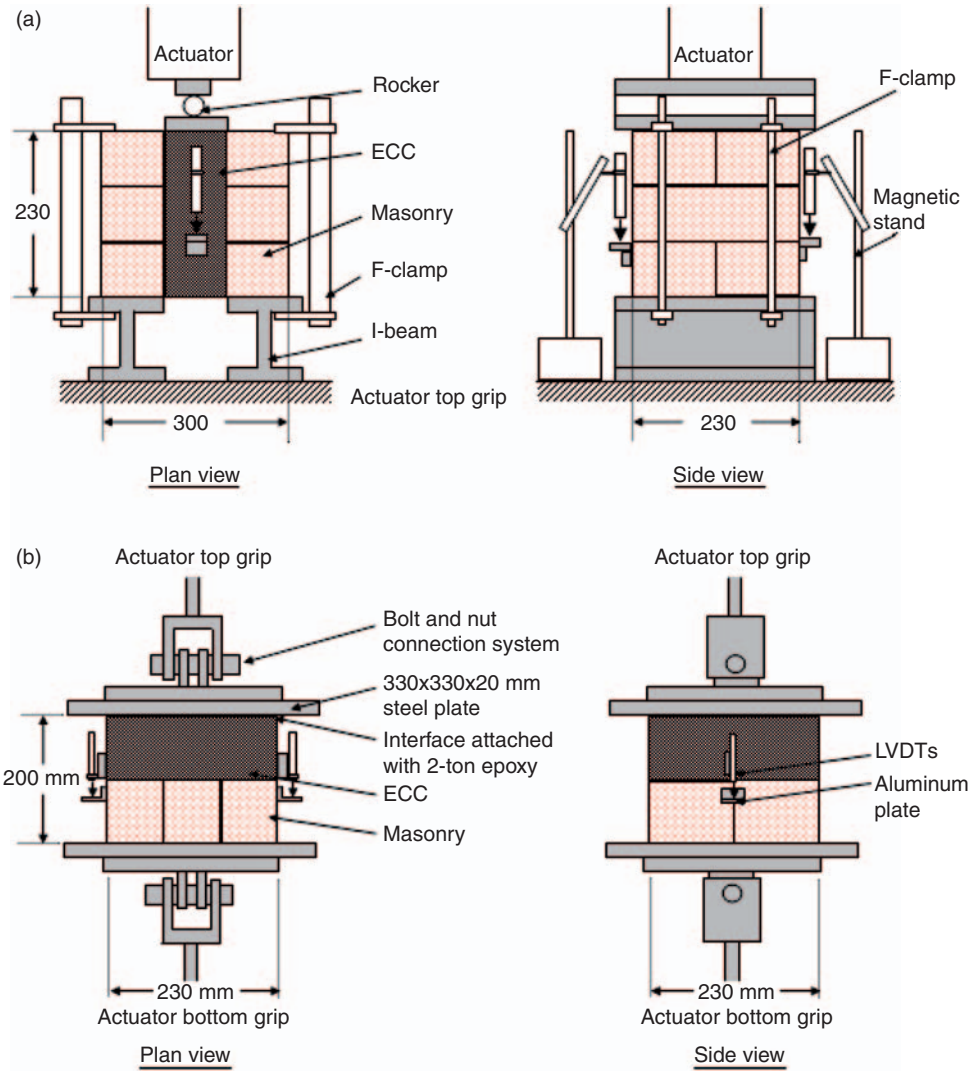

Figure 4. *(a) Plan view and side view of direct shear test, (b) plan view and side view of uni-axial tensile-bond test.*

Experimental Test Set-ups

The test set-ups for both Series I and II were similar except that the loading areas are different as shown in Figure 5(a) and (b), respectively. The test wall was laid horizontal with the reinforced face placed on the distal face of the applied load, simply supported along four sides on round steel bar supports without edge restraint. This means that the corners of the test wall are free to uplift. The effective span of the panel in both directions was 900 mm.

For Series I test, a patch load of 100 mm × 100 mm was applied at the center of the test wall through a spherical seated platen by means of a hydraulic jack head. The load was applied using displacement control hydraulic jack at a constant rate of 0.1 mm/min.

Table 2. Summary of test specimens.

Reinforcing configuration	Steel ratio (%)	Wall thickness (mm)	Remarks	
SE34	0.127	134	34 mm HFECC w/o steel mesh	
DE34	0.202	168	34 mm HFECC w/o steel mesh	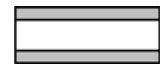
SD8	0.502	134	34 mm HFECC w/ Ø8 steel mesh @ 100 mm spacing	
DD8	0.810	168	34 mm HFECC w/ Ø8 steel mesh @ 100 mm spacing	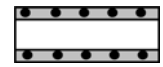

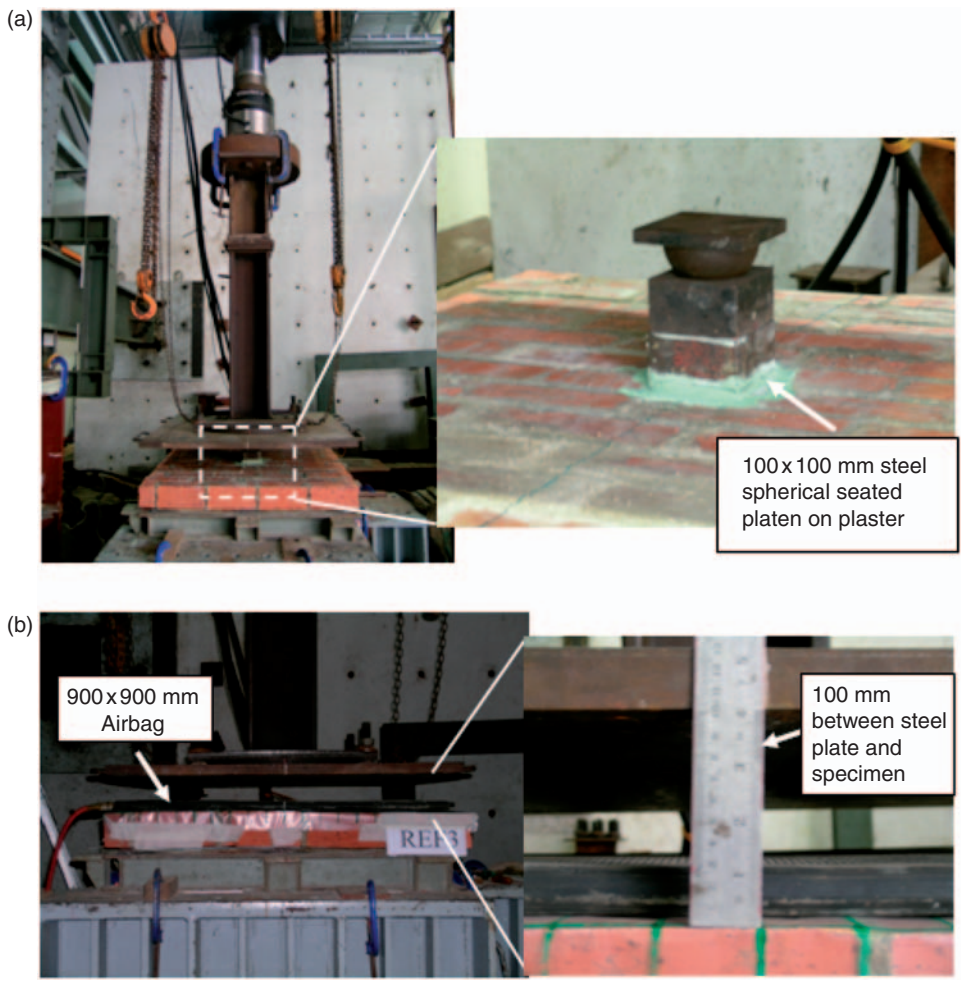

Figure 5. *(a) Series I – patch loading test set-up, (b) Series II – uniformly distributed loading test set-up.*

For Series II test, a UDL of 780 mm × 780 mm was applied at the center of the test wall using a Kevlar reinforced airbag of size 900 mm × 900 mm. The airbag was placed in between a 25 mm thick steel plate of dimension 950 mm × 950 mm (attached to the hydraulic jack head) and the test wall. The distance between the steel plate and the test wall was kept constant at 100 mm throughout the test to minimize changes in the loading area while the airbag was inflated. Gridlines were drawn on the test specimen to monitor the changing load area due to the deformation of the airbag. The loading rate was controlled by the inflation of the airbag at approximately 1.5 kN/min.

To capture the global displacement of the wall panel, five 100 mm-capacity LVDTs were attached to the underside of the test wall. The first LVDT was placed directly under the load, at the center of the test specimen and the remaining four spaced 250 mm away from the center LVDT along both orthogonal directions. The displacement profiles plotted against applied load were used to assess the performance of the different HFECC-strengthening configurations.

EXPERIMENTAL RESULTS AND DISCUSSION

Auxiliary Material Properties Test Results

The mechanical properties of the various materials constituting the HFECC-strengthened walls are summarized in Table 3. Large variations of the tensile strain capacities of HFECC material were observed. Higher tensile strain capacities were observed in specimens with saturated multiple micro-cracks, while lower tensile strain capacities were observed in specimens with localized multiple micro-cracks. The lower bound values

Table 3. Summary of material properties tests.

	Compressive tests			
	No. of specimen	**Compressive strength (MPa)**	**Ultimate strain (%)**	**Elastic modulus (GPa)**
Masonry				
Normal direction	3	21.74	0.33	9.70
Parallel direction	3	15.88	0.33	7.65
Out-of-plane comp.	6	21.26	-	-
HFECC				
Cylinder	3	53.64	0.45	19.50
	Tensile tests			
HFECC coupon	No. of specimen	Tensile strength (MPa)	Ultimate strain (%)	
	6	3.5–4.0	2.1–4.0	
	HFECC-masonry bond tests			
	No. of specimen	Bond strength (MPa)		
Shear	5	1.8		
Uni-axial tensile	5	0.6		

were caused by nonuniform distribution of the fiber reinforcements that resulted in localized failure of the tensile coupons.

In view of the observed saturated multiple micro-cracking pattern and large cross-sectional area of the HFECC-strengthening layer (1000 mm × 34 mm) that could possibly result in better stress re-distribution such that global failure would constitute the dominant test walls' failure mechanism, the upper bound values of HFECC tensile strain were adopted for the theoretical prediction of the walls' ultimate load-carrying capacity.

It is also interesting to note that the relationship for the compressive strength and elastic modulus between the clay masonry's normal and parallel directions are given by:

$$f_c^p = 0.73 f_c^n, \tag{1}$$

$$E_c^p = 0.79 E_c^n, \tag{2}$$

respectively, which agreed reasonably well with relations of concrete masonry obtained from the existing literature [16,17] which are given by:

$$f_c^p = 0.7 f_c^n, \tag{3}$$

$$E_c^p = 0.8 E_c^n, \tag{4}$$

where f_c^p and f_c^n are the compressive strengths of the masonry in the parallel and the normal directions, respectively, E_c^p and E_c^n the elastic moduli of the masonry in the parallel and the normal directions, respectively.

Test Wall Results

The load deflection responses of Series I and II test walls are shown in Figure 6(a) and (b), respectively and their numerical results are summarized in Table 4.

Test Walls Failure Modes and Characteristics

From the load deflection responses graphs, it can be observed that HFECC-strengthening systems improved the performance of URM walls in many aspects. The ultimate load-carrying capacity, deflection, and energy absorption capacity of the URM wall were increased significantly with the HFECC-strengthening systems. The energy absorption capacities were calculated based on the area under the graph up to 90% of the post-ultimate load. Four different failure modes were observed from the experimental tests. They are, (a) tensile flexure failure, (b) compressive flexural failure, (c) punching shear failure, and (d) shear de-bonding of HFECC-strengthening layer(s).

Tensile flexure failures were observed in all URM wall panels. As mentioned earlier, masonry walls are generally designed to withstand compressive stresses. URM walls are primarily made up of discrete brick elements bonded together by intermediate mortar layers. As such, when subjected to out-of-plane loading, the weak interfacial bond between the brick and the mortar layers usually governs the load-carrying capacity of the URM walls, which constituted the observed sudden tensile flexural failure mode. When these URM walls were strengthened with HFECC material, its tensile capacity was increased substantially and this in turn increased its load-carrying capacity and more importantly, changed the brittle tensile failure mode to other ductile failure mechanisms.

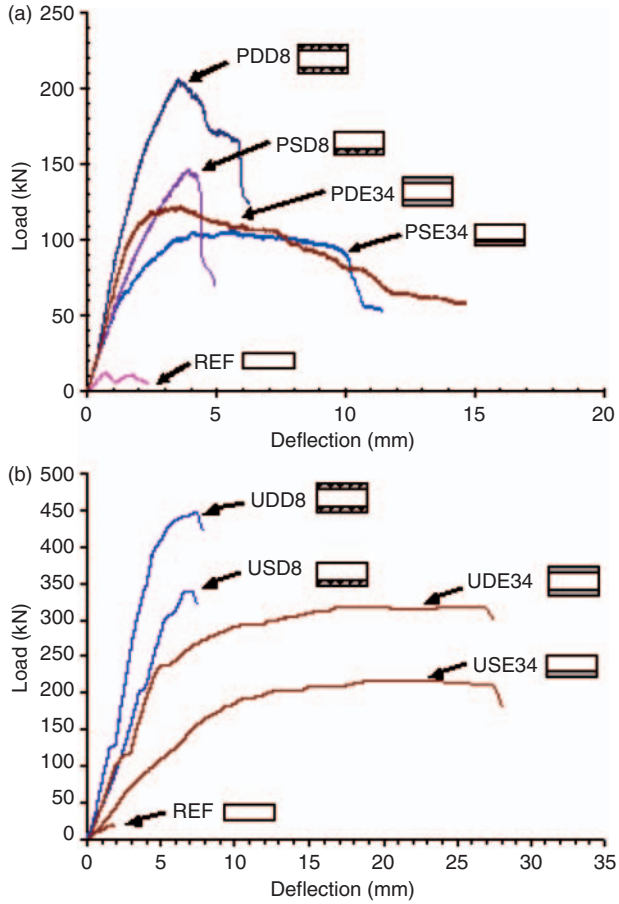

Figure 6. *Load deflection responses of: (a) Series I test walls (b) Series II test walls.*

Table 4. Summary of Series I and II test results.

Specimen	Failure mode	Ultimate load capacity (kN)	Deflection at 90% post-ultimate load (mm)	Energy absorption capacity (J)
Series I tests				
REF	Tensile flexure	11.94	0.74	5.28
PSE34	Compressive flexure	105.52	9.60	836.92
PDE34	Compressive flexure	122.70	5.44	521.97
PSD8	Punching shear	146.88	4.35	398.61
PDD8	De-bonding	206.56	4.53	621.90
Series II tests				
REF	Tensile flexure	20.37	1.73	17.81
USE34	Compressive flexure	217.86	27.53	3265.34
UDE34	Compressive flexure	318.32	27.01	4977.91
USD8	De-bonding	337.32	7.22	944.51
UDD8	De-bonding	447.26	7.43	1456.14

Compression flexural failure was observed in both single-face reinforced and double-face reinforced HFECC-strengthened masonry walls without steel mesh. In the case of the single-face reinforced walls (SE34), the compressive flexural failure occurred owing to the superior tensile strain capacity of HFECC material (up to 4%) as compared to the small ultimate compressive strain capacity of masonry element ($\approx$0.3%). Under the applied loading, the reinforced wall panel experienced bending moment and strain at the extreme fibers increased. Due to the superior strain capacity of HFECC material over masonry material, the ultimate compressive strain of the masonry were exceeded before the HFECC layer fails in tension, hence resulting in the crushing of the top masonry region.

On the other hand, in the case of the double-face reinforced walls (DE34), the compressive failure was due to the buckling of the top HFECC layer. Considering a cross-section of the double-face strengthened wall panel subjected to bending, as the compressive strength of HFECC material (53 MPa) is much higher than its tensile strength (4.8 MPa), only a thin section of the top HFECC layer were subjected to compressive stress (to balance the tensile force), resulting in buckling cum bond failure of the thin HFECC layer. In the case of patch loading, as the de-bonded area of the top HFECC layer increases, the load-carrying capacity of the double-face reinforced wall (PDE34) decreases and it eventually behaved like a single-face reinforced wall (as shown in Figure 6(a)), as the PDE34 curve cuts through the PSE34 curve. However, in the case of UDL, the large loading area enhanced the integral action of the plate and thus contributed to the increased load-carrying capacity of UDE34 as compared to USE34 as shown in Figure 6(b).

Punching shear failure was observed in PSD8, a single-face HFECC-strengthened wall with steel mesh subjected to the patch load. From Figure 6(a), it was observed that the addition of steel mesh reinforcement in the strengthening configuration stiffened the single-face reinforced specimen making it harder to deform compared to PSE34. This inability to deform resulted in high shear stress concentration around the small patch load area. Due to the brittle nature of the masonry material, the instance when the applied load exceeds its punching shear capacity, punching failure takes place without delay, penetrating through the masonry layer and subsequently de-bonding the HFECC layer.

Interfacial de-bonding failure of the strengthening layers was observed in masonry walls strengthened with HFECC and steel mesh reinforcements. In these strengthening configurations, the steel mesh made the HFECC-strengthening layers very stiff and therefore harder to deform as mentioned earlier. When the applied load is high, large shear stresses develop along the HFECC-masonry interface builds up due to the differential deformation of the masonry and HFECC layers, which eventually cause them to de-bond.

To summarize the above discussions, HFECC-strengthening systems that consist of steel mesh reinforcements possess higher ultimate load-carrying capacities, but with lesser ductility. This is because the additional steel mesh makes the composite panel stiffer, thus giving it a higher strength but at the same time reduces its ability to deform. Hence, depending on the objective of the application, different reinforcing configuration may be employed to achieve the required performance of the masonry structures.

HFECC-strengthening Layer Crack Patterns

A typical crack pattern of a HFECC-strengthening layer without steel mesh reinforcement is shown in Figure 7(a). The HFECC layer displayed very good stress distribution, having well-distributed cracks beneath the loading area stretching out towards the support in a radial pattern. For the HFECC layer reinforced with additional 8 mm diameter steel

mesh, the cracks are less dense as shown in Figure 7(b). This observation indicates that the stresses were mostly distributed through the steel mesh instead of the HFECC layer. In addition, as the steel mesh was pressing against the HFECC layer, the shape of the steel mesh was visible from the crack pattern.

Cost Analysis of HFECC-strengthening System and GFRP-Strengthening System

Omitting labor (as this is country-dependent) and material shipping cost, a material cost analysis (correct as at January 2008) for HFECC-strengthening system and glass fiber-reinforced polymer (GFRP)-strengthening system for a 1000 mm × 1000 mm masonry wall was conducted and the detail material breakdown costs (in US dollars) are shown in Table 5. GFRP-strengthening system costs $95.81 USD while HFECC-strengthening system costs only $22.94 USD, which is four times cheaper than the former. Therefore, it will be more practical and economical for civilian structures to be retrofitted with HFECC-strengthening system.

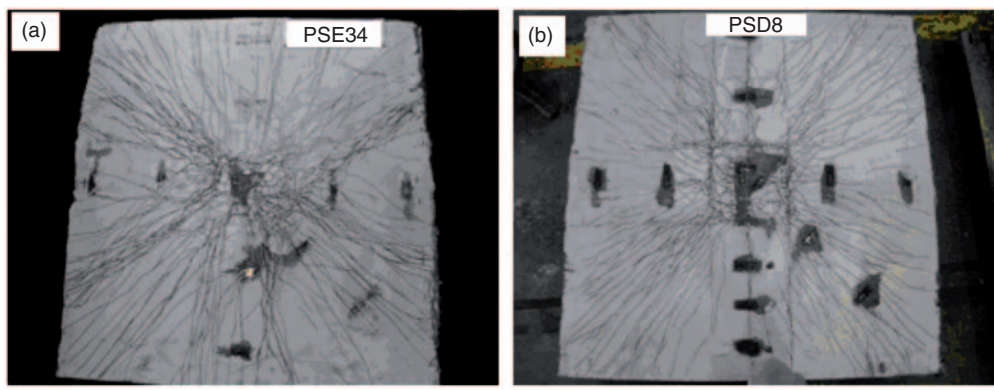

Figure 7. *Typical cracking pattern of HFECC-strengthening layer: (a) without steel mesh (b) with steel mesh.*

Table 5. Material breakdown costs for HFECC- and GFRP-strengthening systems.

	Material	Cost/Unit	Quantity	Cost
	HFECC-strengthening system			
1	Cement	$0.097/kg	28.00 kg	$2.72
2	Silica fume	$1.06/kg	3.80 kg	$4.03
3	Superplasticizer	$1.32/L	0.40 L	$0.53
4	Polyethylene (PE) fiber	$41.23/kg	0.29 kg	$11.96
5	Steel (ST) fiber	$4.74/kg	0.78 kg	$3.70
			Total	$22.94
	FRP-strengthening system			
1	GFRP (4 layers)	$9.93/m^2	4.00 m^2	$39.72
2	MBrace primer (1 layer)	$9.27/kg	0.23 kg	$2.13
3	MBrace putty (1 layer)	$5.96/kg	4.34 kg	$25.87
4	MBrace saturant (4 layers)	$9.27/kg	3.03 kg	$28.09
			Total	$95.81

ANALYTICAL MODELS FOR HFECC-STRENGTHENED WALLS

Derivation of Simplified Analytical Models

As mentioned earlier, three failure mechanisms were observed from the HFECC-strengthened masonry walls. They are namely, (a) flexural failure, (b) punching shear through the bricks, and (c) shear de-bonding of the HFECC-layer. Simplified analytical models were derived to predict the ultimate load-carrying capacities of the HFECC-strengthened walls based on these observed failure mechanisms.

FLEXURAL FAILURE

The moment capacity for the HFECC-strengthened masonry wall was derived based on strain compatibility and constitutive relationship, similar to that used for a reinforced concrete member. Assuming plane section remains plane after bending, a linear strain distribution across the section is obtained. In view that the tensile resistance of brick masonry being smaller compared to that of HFECC-strengthening layer (and becomes negligible when cracks occur through the section), it is ignored in the analysis.

The tensile strength of HFECC material was assumed to be a constant (=ultimate tensile strength) when its strain value exceeds 0.5%, while the actual parabolic stress—strain relationship of the brick masonry was simplified by substituting an equivalent rectangular compressive stress block, with stress intensity of $k_1 f_{wcu}$ over a depth of x [18], where f_{wcu} is the ultimate compressive strength of the brick masonry and x is the neutral axis depth as shown in Figure 8. The constant k_1 can be determined through the following expression

$$k_1 = \frac{\varepsilon_u}{\varepsilon_m} - \frac{1}{3}\left(\frac{\varepsilon_u}{\varepsilon_m}\right)^2 \tag{5}$$

where ε_u and ε_m are the ultimate and maximum compressive strain of the masonry, respectively, which was found to be 0.0033 and 0.003, respectively from the experimental tests. Substituting the values into Equation (5), the constant k_1 can be approximate to be 0.697.

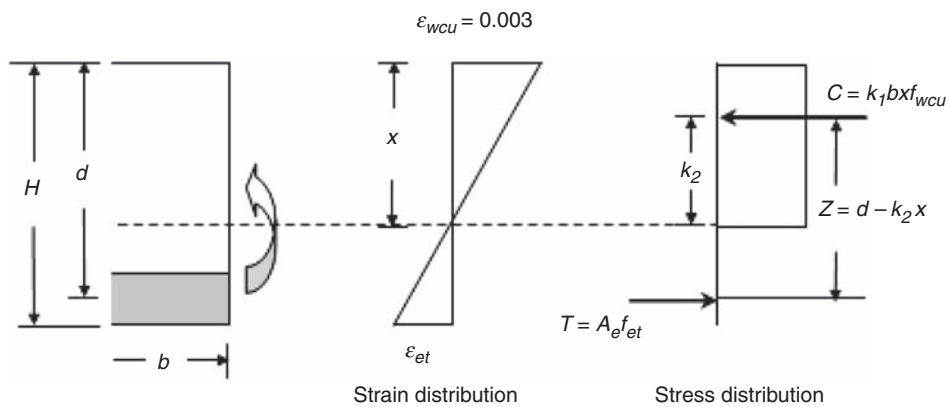

Figure 8. *Section analysis for flexural failure.*

The location of the resultant compressive force, C, acting on the masonry section is given by k_2x, where k_2 is expressed as

$$k_2 = \left[4 - \left(\frac{\varepsilon_u}{\varepsilon_m}\right)\right] \Big/ \left[12 - 4\left(\frac{\varepsilon_u}{\varepsilon_m}\right)\right]. \tag{6}$$

Similarly, based on the experimental test results, the constant k_2 is found to be 0.382.

Consider the simplest case of a section of the brick masonry reinforced with a single layer of HFECC material without steel mesh (SE34), with width b and thickness H, subjected to bending moment as shown in Figure 8, the ultimate moment capacity of the SE34 strengthened masonry wall can therefore be obtained as:

$$M_u = k_1 b x f_{wcu} Z, \tag{7}$$

where Z is the moment lever arm, taken as $(=d - k_2x)$. The neutral axis depth at failure can be determined through force equilibrium, by equating the tensile and compressive forces to obtain the following expression:

$$x = \frac{A_e f_{et}}{k_1 b f_{wcu}}, \tag{8}$$

where A_e is the cross-sectional area of the HFECC-layer and f_{et} the tensile strength of HFECC material. Similarly, for any other reinforcing configurations, the ultimate load-carrying capacity as well as the neutral axis depth can be determined through iterations by balancing the tensile and compressive forces.

PUNCHING SHEAR FAILURE

In the design of masonry walls, in-plane compressive failures have been the main concerns and hence, limited number of studies were carried out on the out-of-plane punching shear failure of masonry walls. In a previous study [19] carried out on FRP-reinforced masonry walls, a theoretical model for the punching shear failure of reinforced concrete (RC) was modified for the use of FRP-strengthened masonry walls and it matched reasonably well with experimental results. Similarly, in this present study, the HFECC-strengthened masonry wall was considered as analogous to a steel RC slab and an attempt was made to adapt the existing BS8110 code [20] equation for the punching shear strength of a RC slab, which is given by:

$$P_u = v_u u d \leq 0.8\sqrt{f_{cu}} u_o \mathrm{d}, \tag{9}$$

in which u is the critical punching shear perimeter, taken to be $1.5d$ from the periphery of the loaded area, that is $u = 2(l_x + l_y + 6d)$, l_x and l_y are the length and breadth of the loaded area, respectively and d is the effective depth of the slab. The design shear stress, v_u is given by:

$$v_u = 0.79\left(\frac{100A_s}{bh}\right)^{\frac{1}{3}}\left(\frac{400}{d}\right)^{\frac{1}{4}}, \tag{10}$$

where A_s is the area of steel reinforcement, b is the width of the section considered and h is the height of the section. For a concrete compressive strength, f_{cu}, greater than 25 MPa, v_u may be multiplied by a factor of $\sqrt[3]{f_{cu}/25}$. However, the value of f_{cu} should not be greater than 40 MPa.

Equations (9) and (10) were modified for the use of HFECC-strengthened masonry walls by considering an equivalent reinforcement ratio and adjusting the critical punching

shear perimeter. Using the concept of equivalent area transformation, the area of HFECC, A_e, can be transformed to an equivalent area of steel, A_{es}, by:

$$A_{es} = \frac{E_e}{E_s} A_e, \tag{11}$$

where E_e and E_s are the elastic modulus of HFECC and steel, respectively.

The critical punching shear perimeter observed from the experimental test was smaller than the perimeter suggested by the BS8110 code. The critical perimeter was approximately $0.6d$ from the periphery of the loaded area as shown in Figure 9, and it can be represented by:

$$u = 2(l_x + l_y + 2.4d). \tag{12}$$

In addition, as the punching failure did not punch through the ductile HFECC-layer, the punching depth should only be taken as the thickness of the masonry wall, h, instead of the effective depth, d. By incorporating the above modifications and by replacing f_{cu} with the out-of-plane compressive strength of the brick masonry (f^o_{mc}), the punching shear failure load for a HFECC-retrofitted masonry panel can be derived as:

$$P_u = 1.58\left(\frac{100A_s}{bh}\right)^{\frac{1}{3}}\left(\frac{400}{d}\right)^{\frac{1}{4}}(l_x + l_y + 2.4d)h. \tag{13}$$

SHEAR DE-BONDING FAILURE

The shear-bond failure leading to de-bonding of HFECC-strengthened masonry wall was estimated by considering the normal and shear stress distributions across the cross-section of the reinforced panel as shown in Figure 10, which can be determined using the following expressions:

$$\sigma = -\frac{My}{I_c}, \tag{14}$$

$$\tau = \frac{VA'\overline{y}}{I_c b}, \tag{15}$$

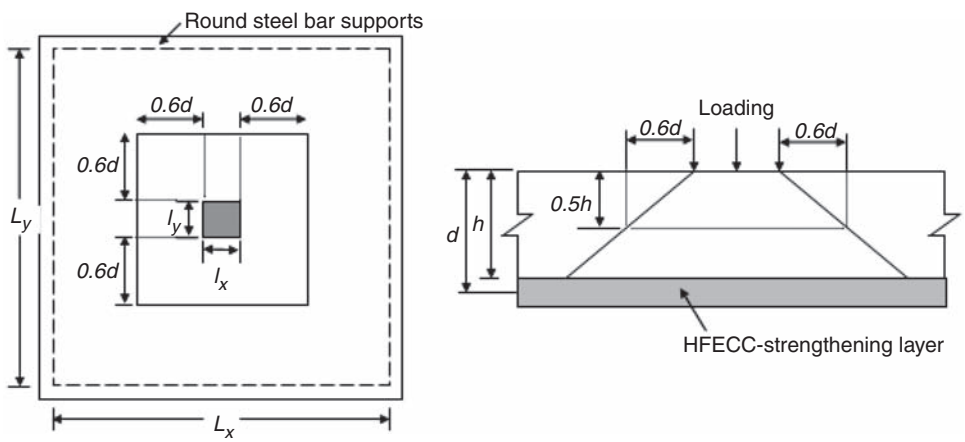

Figure 9. *Observed critical punching shear perimeter.*

where M and V are the moment and shear force at the considered section, respectively, y is the distance between the point of interest and neutral axis, I_c the composite second moment of area of the section, A' the area of section from the point of interest towards bottom of the section, $\overline{y}$ the distance from the centroid of A' to the neutral axis, and b the width of the section. It should be noted that A' is multiplied by an area transformation factor if the material properties are different from that used to calculate the second moment of area.

Shear-bond failure occurs when the combined stresses at the HFECC-masonry interface induced by shear force and bending moment exceeds the HFECC-masonry interfacial shear strength, τ_u (=1.8 MPa as obtained from the experimental tests). The critical combination and location of the normal and shear stresses is dependent on the structural loading configurations. In the case of a simply supported beam subjected to a point load at the mid-span, the critical combination of stresses would be found at the mid-span of the beam (refer to Appendix A for detail calculations). Thus, the shear-bond failure load can be determined using the following expression:

$$P = \frac{2\tau_u I_c}{(yL/2) + (A'\overline{y}/b)}, \tag{16}$$

where P is the ultimate load-carrying capacity of the HFECC-strengthened beam and L is its effective length. As for other loading configurations, analysis should be performed

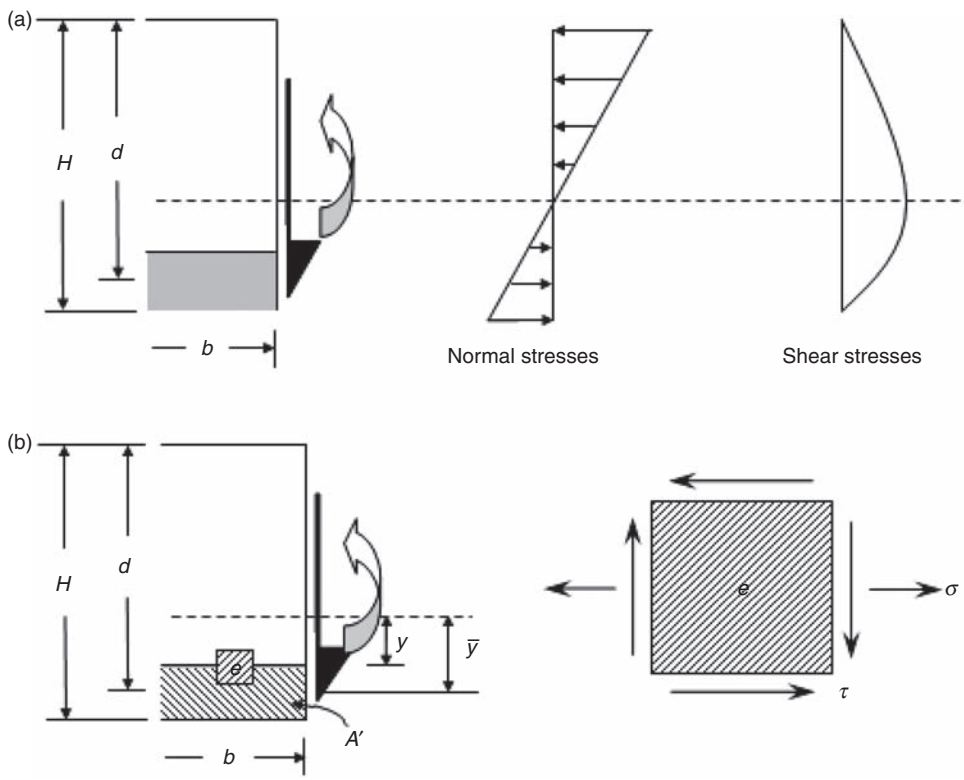

Figure 10. *(a) Normal and shear stresses distribution, (b) element extracted from section subjected to normal and shear stresses.*

at several locations across the span of the beam to determine the critical combination of the shear and normal stresses, which would yield the lowest load-carrying capacity of the wall.

ULTIMATE LOAD-CARRYING CAPACITY OF HFECC-STRENGTHENED WALLS

The analytical models for flexural and shear de-bonding failures derived earlier were based on taking a strip of the panel in one direction. To obtain the out-of-plane ultimate load-carrying capacity of the panel, consider a simply supported wall, measuring L_x and L_y in x and y directions, respectively, subjected to a patch load at the center over a rectangular area of dimensions l_x by l_y as shown in Figure 11(a).

It should be noted that the assumption of zero deflection ($w = 0$) along the edges of the so-called simply supported panel is physically not correct [21]. Due to the deflection of the panel and the torsion effects, the corners of the panel will lift up.

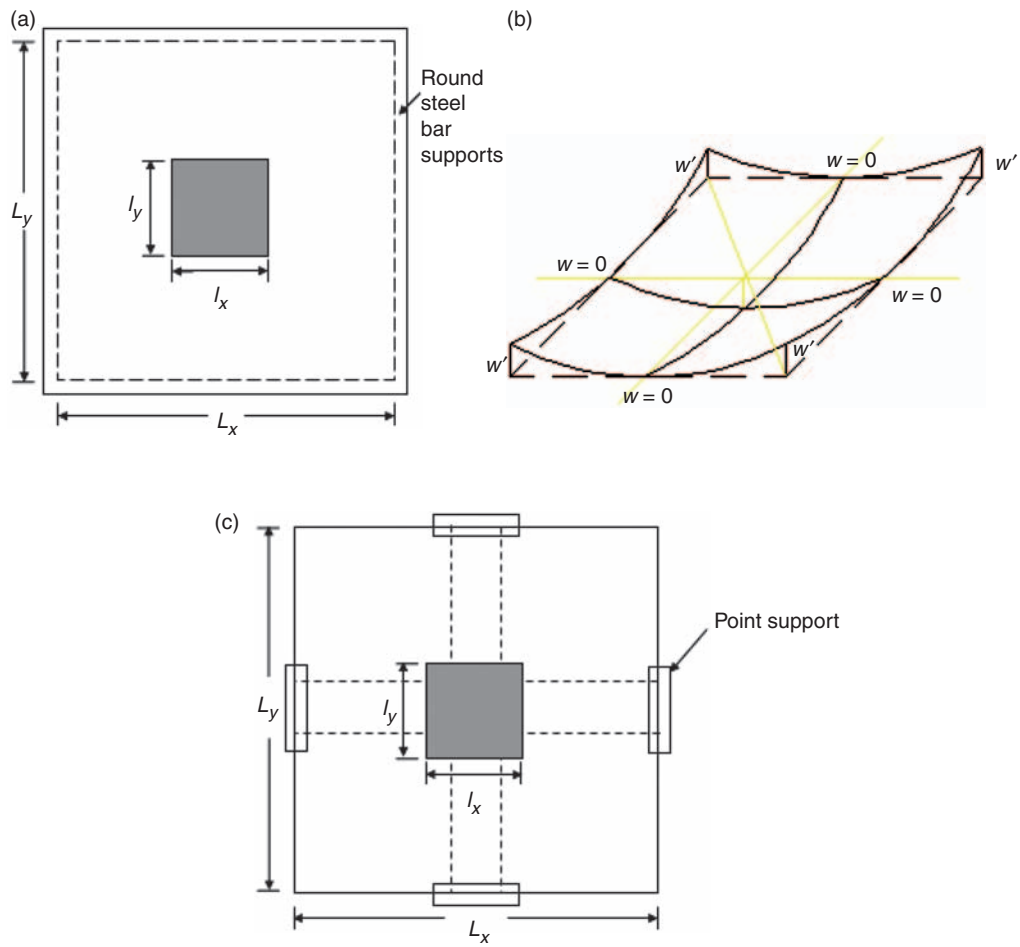

Figure 11. *(a) Plan view of experimental set-up, (b) uplifting at the corners, (c) panel resting on four-point supports.*

Unless special structural provisions are made, the deflection pattern shown in Figure 11(b) will generally occur and therefore, the panel will be resting on four points as shown in Figure 11(c).

Using the strip method theory [22], the panel was divided into two systems of strips orthogonal to one another, each functioning in the beam mode to carry the imposed load. For the loaded system of beams to function as a panel, the following conditions must be met. Firstly, the mid-span deflection of the two orthogonal strips must be equal and secondly, the sum of the load resisted by the individual beam system must be equal to the total load applied to the panel. These conditions can be expressed as:

$$w_{L_x/2} = w_{L_y/2}, \tag{17}$$

$$P_u = P_x + P_y, \tag{18}$$

where $w_{L_x/2}$ and $w_{L_y/2}$ are the mid-span deflections of the strip in x and y directions, respectively, P_x and P_y the load resisted by the strip in x and y directions, respectively.

In the case of a panel with simply supported edges and subjected to a uniform distributed load, the deflections at the mid-span of the strips are given by:

$$w_{L_x/2} = \frac{5P_xL_x^4}{384E_xI_x}, \tag{19}$$

$$w_{L_y/2} = \frac{5P_yL_y^4}{384E_yI_y}, \tag{20}$$

where E_x and E_y are the elastic modulus of the section in the x and y directions, respectively, I_x and I_y the second moment of area in the x and y directions, respectively. By incorporating the governing conditions, we can determine the load resisted by each strip as:

$$P_x = P_u \frac{E_xI_x}{E_yI_y} \frac{L_y^4}{L_x^4 + L_y^4}, \tag{21}$$

$$P_y = P_u \frac{E_yI_y}{E_xI_x} \frac{L_x^4}{L_x^4 + L_y^4}, \tag{22}$$

and the ultimate load-carrying capacity of the masonry panel as:

$$P_u = P_x \frac{E_yI_y}{E_xI_x} \frac{L_x^4 + L_y^4}{L_y^4} = P_y \frac{E_xI_x}{E_yI_y} \frac{L_x^4 + L_y^4}{L_x^4}. \tag{23}$$

The above method to obtain the ultimate load-carrying capacity of the reinforced masonry wall closely simulates the actual experimental boundary condition, which was a four-point simply support case as mentioned earlier. This derived relationship is also able to account for the orthogonal properties of the masonry wall. However, as this

relationship is derived based on elastic theory, some discrepancies between the simplified solution and that from experiments are to be expected.

In addition, the boundary condition assumed a strip smaller than the actual width of the slab and thus may underestimate the ultimate load-carrying capacity of the panel compared to that from classical plate theory. For instance, the ultimate load-carrying capacity of an isotropic square slab, simply supported along its perimeter, using the above-illustrated method is $16M_u/l^2$, while the value determined using classical plate theory is $21.3M_u/l^2$, thus under-predicting by 25%. However, if the panel corners do lift, then a value below the classical value of $21.3M_u/l^2$ will be reasonable.

Comparison of Theoretical and Experimental Results

The ultimate load-carrying capacities of the HFECC-strengthened walls are determined using the derived analytical models and material properties obtained from the experimental tests, and those of the URM walls are determined through elastic section analysis and assuming the ultimate tensile strength of URM to be 5% of its ultimate compressive strength. The predicted values of the HFECC-strengthened walls are compared with those obtained experimentally, as shown in Table 6.

The theoretical predicted results were observed to match favorably with experimental results, with ratios of experimental to theoretical values ranging from 0.92 to 0.96 for flexural failure, 1.00 for punching shear failure and 0.95 to 0.97 for shear de-bonding failure.

However, for PDE34 and UDE34, the derived analytical models could not predict the failure load as the failure mode was not exactly the typical crushing of the top HFECC-strengthening layer as discussed earlier. Nevertheless, by performing section analysis at small strain-steps for PDE34, it can be shown that the neutral axis of the reinforced wall is only 16.2 mm when the applied load is approximately 120 kN. Likewise for UDE34, it can be shown that the neutral axis of the reinforced wall is only 13.6 mm when the applied load is approximately 320 kN, both suggesting that buckling failure could have occur when the small thickness of the HFECC layer was subjected to high compressive stresses.

SUMMARY AND CONCLUSIONS

HFECC material was successfully used to strengthened masonry walls against out-of-plane loadings, in which significant improvements of the wall performance, in terms of load-carrying capacity (up to 22 times), ductility (up to 16 times), and energy absorption capacity (up to 280 times) were observed. Addition of steel mesh reinforcement within the HFECC-strengthening layers generally increased the walls' load-carrying capacity (ranging from 40% to 68%), but at the expense of compromising its ductility (ranging from 17% to 74%) compared to those of HFECC-strengthened wall without steel mesh. Based on the observed failure mechanisms, analytical models to predict HFECC-strengthened walls' ultimate load-carrying capacity were derived and favorable results between the theoretical values and the experimental data were observed.

Table 6. Summary of theoretical predictions and experimental results.

Specimen	Theoretical predicted failure load (kN)			Observed failure	Experimental failure load (kN)	Experimental/ Theoretical ratio
	Flexure (C/T)[a]	Punching Shear	De-bonding			
Series I tests						
REF	12.71 (based on elastic sectional analysis)			Tensile flexure	11.94	0.94
PSE34	114.90 (C)	139.71	145.00	Compressive flexure	105.52	0.92
PDE34	194.32 (T)	N.A.	200.63	Compressive flexure	122.70	–
PSD8	327.71 (C)	146.44	163.53	Punching	146.88	1.00
PDD8	511.62 (C)	N.A.	222.53	De-bonding	206.56	0.95
Series II tests						
REF	21.19 (based on elastic sectional analysis)			Tensile flexure	20.37	0.96
USE34	212.28 (C)	N.A.	295.29	Compressive flexure	217.86	0.96
UDE34	361.08 (T)	N.A.	406.45	Compressive flexure	318.32	–
USD8	546.18 (C)	N.A.	348.87	De-bonding	337.32	0.97
UDD8	852.70 (C)	N.A.	462.93	De-bonding	447.26	0.97

[a](C) for compressive and (T) for tensile flexural failure.

APPENDIX A

Figure A1 shows a simply support beam subjected to a point load. Both maximum moment and shear force occurs at the mid-span of the beam. Therefore, the critical combination of the normal stress and shear stress will also be found at the mid-span given by the following, respectively, as:

$$\sigma = -\frac{My}{I_c} = -\frac{PLy}{4I_c}, \tag{A1}$$

$$\tau = \frac{VA'\overline{y}}{I_c b} = \frac{PA'\overline{y}}{2I_c b}. \tag{A2}$$

Shear-bond failure will occurs when the sum of these two stresses is greater than the HFECC-masonry interfacial shear strength, τ_u, which can be re-arrange to be expressed in terms of the beam ultimate load-carrying capacity given as:

$$P_u = \frac{2\tau_u I_c}{\frac{yL}{2} + \frac{A'\overline{y}}{b}}. \tag{A3}$$

The above procedures can be repeated to calculate the shear-bond failure load for any other loading type.

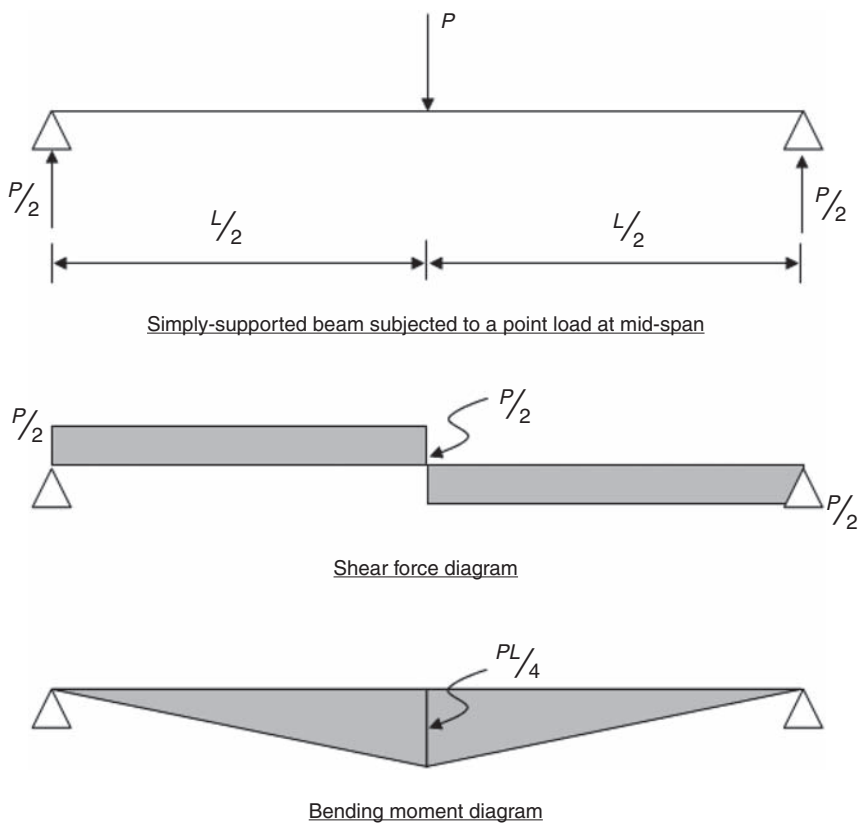

Figure A1. *Simply supported beam subjected to point load.*

REFERENCES

1. Wenzel, F. (1989). On the Structural Repair of Masonry, In: Brebbia, C.A. (ed.), *Structural Repair and Maintenance of Historical Buildings*, pp. 83–94, Computational Mechanics Publications, Southampton, Boston.
2. Ehsani, M.R. (1995). Strengthening of Earthquake-Damage Masonry Structures with Composite Materials, In: Taerwe, L. (ed.), *Non-metallic (FRP) Reinforcement for Concrete Structures*, pp. 680–687, Spon, London.
3. Triantafillou, T.C. (1998). Strengthening of Masonry Structures Using Epoxy-Bonded FRP Laminates, *Journal of Composites for Construction, ASCE*, **2**(2): 96–104.
4. Gilstrap, J.M. and Dolan, C.W. (1998). Out-of-Plane Bending of FRP-Reinforced Masonry Walls, *Composite Science and Technology*, **58**: 1277–1284.
5. Li, V.C. (1998). Engineered Cementitious Composites – Tailored Composites through Micromechanical Modeling, In: Banthia, N., Bentur, A. and Mufti, A. (eds), *Fiber Reinforced Concrete: Present and the Future*, pp. 64–97, Canadian Society of Civil Engineers, Montreal.
6. Kanda, T. and Li, V.C. (1999). A New Micromechanics Design Theory for Pseudo Strain Hardening Cementitious Composite, *Journal of Engineering Mechanics, ASCE*, **125**(4): 373–381.
7. Kim, J.K., Kim, J.S., Ha, G.J. and Kim, Y.Y. (2007). Tensile and Fiber Dispersion Performance of ECC (Engineered Cementitious Composites) Produced with Ground Blast Furnace Slag, *Cement and Concrete Research*, **37**: 1096–1105.
8. Li, V.C. and Kanda, T. (1998). Engineered Cementitious Composites for Structural Applications, *Materials in Civil Engineering*, **10**(2): 66–69.
9. Zhang, J., Maalej, M. and Quek, S.T. (2004). Hybrid Fiber Engineered Cementitious Composites (ECC) for Impact and Blast-Resistant Structures, In: *Proceedings of First International Conference on Innovative Materials and Technologies for Construction and Restoration–IMTCR04*, Lecce, pp. 136–149.
10. Li, V.C., Dhanada, K.M. and Wu, H.C. (1995). Matrix Design for Pseudo-Strain-Hardening Fiber Reinforced Cementitious Composites, *Journal of Materials and Structures, RILEM*, **28**(183): 586–595.
11. Maalej, M., Quek, S.T. and Zhang, J. (2005). Behavior of Hybrid-Fiber Engineered Cementitious Composites Subjected to Dynamic Tensile Loading and Projectile Impact, *Journal of Material in Civil Engineering, ASCE*, **17**(2): 143–152.
12. Ahmed, S.F.U. (2003). Corrosion Durability and Structural Response of Functionally-graded Concrete Beams, PhD Thesis, National University of Singapore.
13. Li, M. and Li, V.C. (2006). Behaviour of ECC/Concrete Layered Repair System under Drying Shrinkage Conditions, *Journal of Restoration of Buildings and Monuments*, **12**(2): 143–160.
14. ASTM C 469-02 (2002). *Standard Test Method for Static Modulus of Elasticity and Poisson's Ratio of Concrete in Compression*, ASTM International, West Conshohocken, PA (www.astm.org).
15. BS5628 (1992). *Code of Practice for the Use of Masonry, Part 1*, British Standards Institution, London.
16. Dawe, J.L. and Seah, C.K. (1989). Out-of-plane Resistance of Concrete Masonry Infilled Panels, *Canadian Journal of Civil Engineering*, **16**: 854–864.
17. Dawe, J.L., Liu, Y. and Seah, C.K. (2001). A Parametric Study of Masonry Infilled Steel Frames, *Canadian Journal of Civil Engineering*, **28**: 149–157.
18. Hendry, A.W. (1991). *Reinforced and Prestressed Masonry*, Longman Scientific & Technical, New York.

19. Patoary, M.K.H. (2003). Strengthening of Masonry Walls against Out-of-Plane Loads Using FRP Systems, PhD Thesis, National University of Singapore.
20. BS8110 (1998). *Structural use of Concrete, Parts 1–3*, British Standards Institution, London.
21. Florin, G. (1980). *Theory and Designs of Surface Structures – Slabs and Plates*, pp. 193–194, Trans Tech Publications, West Germany.
22. Ugural, A.C. (1999). *Stress in Plates and Shells*, **2nd edn**, pp. 168–171, The McGraw-Hill, USA.